The effect of stepwise image resolution reduction on red blood cell segmentation

Nora Derner

Department of Information Technology

Uppsala University

Uppsala, Sweden

nora.derner.8232@student.uu.se

Abstract—**Accurate red blood cell segmentation is essential for Deep Learning-based malaria diagnostics, as it directly influences parasite classification and spectral analysis. In this study, two Cellpose models were trained on images with systematically reduced resolutions, ranging from `1200x1600` to `60x80` pixels, using manually annotated ground truth cell masks. Segmentation accuracy was evaluated both pixel- and cell-wise through Dice Score, Panoptic Quality Score, and F1 Score. The findings indicate that segmentation accuracy remains stable down to `360x480` pixels but declines significantly beyond this point, with the cell outline quality becoming increasingly rectangular. When comparing the performance of different imaging modes, reflection mode outperforms transmission and scattering modes, possibly due to the ground truth masks being generated from reflection mode. Identifying a low threshold resolution for effective segmentation highlights the potential of Deep Learning based malaria diagnostics, offering a fast and cost-effective solution.**

Index Terms—**Malaria Diagnosis, Multispectral Imaging, Multimodal Imaging, Cell Instance Segmentation, Image Resolution**

I. INTRODUCTION

Malaria is a life-threatening disease caused by Plasmodium parasites, transmitted through the bites of infected Anopheles mosquitoes. It is prevalent in tropical and subtropical regions. The disease presents with flu-like symptoms and can rapidly progress to a fatal outcome within a week if left untreated [21], [27].

There are various diagnostic methods for malaria [17]. The standard approach persists as the manual examination of thin, stained blood smears under a microscope [26]. This process is time-consuming and dependent on the expertise of the clinician. Recent advances in image analysis and machine learning have significantly improved computer-aided and automated malaria diagnosis [8], [15], [22] showing high accuracy and promising potential for point-of-care applications. The emphasis is on enabling rapid on-site diagnosis, as demonstrated by the miLab™ device in [2]. These lightweight Deep Learning (DL) techniques are especially suited for mobile applications due to their reduced computational requirements [6].

The use of DL diagnostic algorithms enables classification of malaria parasites without the need for time-consuming staining of blood smears [14]. In [16], an optical method is introduced that distinguishes by quasi-simultaneously measuring transmission, reflection, and scattering properties using a multispectral and multimodal light-emitting diode microscope developed in [3]. Transmittance reveals cell absorption properties, scattering highlights internal structural characteristics, and reflectance captures details related to the outer shape. [16]. Hemoglobin changes and hemozoin presence in infected red blood cells (RBCs) enable spectroscopic malaria diagnosis [12].

II. PROBLEM STATEMENT

The precise classification of RBCs is based on the correct segmentation of individual cells. Thin blood smears with minimal overlap or touching cells are ideal for optimal segmentation [22]. Traditional segmentation methods like Otsu [22] are being replaced by advanced DL techniques such as Cellpose [25], MaskRCNN [1], [13], and Stardist [23]. In DL-based cell segmentation, higher resolution images improve accuracy but require more resources, while lower resolution images are faster to process but may reduce segmentation quality. Furthermore, lower resolution imaging allows for imaging more cells per field of view, increasing the chances of identifying low levels of malaria infection. Balancing these factors is key to optimizing segmentation and subsequent spectral analysis. This study aims to determine the resolution threshold for acceptable segmentation in malaria diagnosis, evaluating how resolution reduction impacts accuracy across reflection, scattering, and transmission imaging modalities. The following research question is addressed:

How does stepwise reduction in image resolution influence the accuracy of RBC segmentation, and how does this vary between imaging modalities (reflection, scattering, transmission)?

III. METHODOLOGY AND MATERIALS

A. Dataset

The Toy2 dataset (12×5 samples) used in this study was prepared in Yamoussoukro, Ivory Coast [16] and generated with a multispectral multimodal microscope [3]. Each sample was imaged in three modes—reflectance, scattering, and transmission—using 13 monochromatic wavelengths (380–935 nm) across the UV-Vis-NIR spectrum. This resulted in grayscale images with 13 channels at a resolution of `1200x1600` pixels. Images were normalized to reduce noise and illumination variations [19]. A random subsample of 16 normalized samples was selected for this work, as shown in Table I.

Dataset	M1	M2	Files	ROIs	#Images
Train - Train	x	x	T00_Sample1	1020	3x10
	x	x	T01_Sample1	440	3x10
		x	T06_Sample1	836	3x10
		x	T07_Sample5	687	3x10
		x	T10_Sample3	560	3x10
Train - Test	x	x	T04_Sample3	431	3x10
	x	x	T12_Sample2	556	3x10
		x	T11_Sample1	577	3x10
		x	T05_Sample3	707	3x10
		x	T07_Sample5	504	3x10
Eval	x	x	T02_Sample1	634	3x24
	x	x	T03_Sample4	891	3x24
	x	x	T08_Sample2	1059	3x24
	x	x	T09_Sample5	784	3x24
	x	x	T11_Sample3	640	3x24
Test	x	x	T07_Sample1	Unknown	3x10

B. Segmentation Model Selection

Cellpose 2.0 [20] was selected as the segmentation algorithm for this study due to its superior accuracy and robustness compared to Mask R-CNN [13] and StarDist [25].

C. Preprocessing

Since Cellpose requires 3-channel images and was trained on data with a dark background and bright objects, the data subset I undergoes two preprocessing steps:

First, pixel values in the reflectance and transmission modes are inverted to ensure bright objects on a dark background, while scattering mode images, already exhibiting this property, are not inverted. This is done in ImageJ via `Edit > Invert`. Next, the number of channels is reduced from 13 to 3 using ImageJ's `Image > Stacks > Tools > Reduce > Reduction Factor 5`. An example of the images before and after preprocessing is shown in Figure 1.

D. Ground Truth Generation

To evaluate the segmentation model, ground truth files (`masks.png`) were created for all reflection images in the Train and Evaluation Dataset I. Masks were generated only from the reflection mode, which captures outer shape details [16], and reused for transmission and scattering modes. These masks include instance segmentation for cell regions of interest. The Cellpose 2.0 GUI was used for generation, with the model `cyto2_cp3` and a pixel diameter corresponding to the average cell size (40 pixels) determined experimentally. In order to have a correct set of cell masks for training and testing, some cells were incorrectly segmented, and errors were manually corrected by adding or removing regions.

E. Reduction of Image Resolution

To have a multi-resolution dataset for training and testing, a script `resize_tif_png.py` was developed to rescale TIFF images and optional PNG masks. For each scaling factor, the script generates rescaled images and masks, ensuring label integrity through nearest neighbor interpolation for masks and bilinear interpolation for images. Pixel dimensions are shown in Table II.
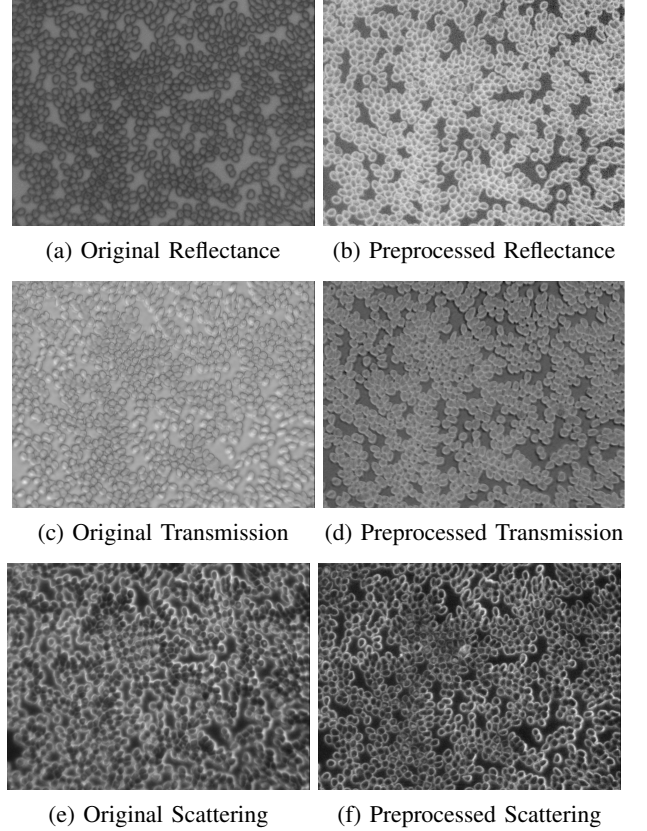
Fig. 1: Preprocessing on T00_Sample1

(a) Original Reflectance

(b) Preprocessed Reflectance

(c) Original Transmission

(d) Preprocessed Transmission

(e) Original Scattering

(f) Preprocessed Scattering

TABLE II: Rescaled image and mask dimensions

| Factor	Image Dim	Mask Dim	Diameter Cell
1.0	1200x1600x3	1200x1600	45
0.9	1080x1440x3	1080x1440	40.5
0.8	960x1280x3	960x1280	36.0
0.7	840x1120x3	840x1120	31.5
0.6	720x960x3	720x960	27.0
0.5	600x800x3	600x800	22.5
0.4	480x640x3	480x640	18.0
0.3	360x480x3	360x480	13.5
0.2	240x320x3	240x320	9.0
0.1	120x160x3	120x160	4.5

F. Cellpose Model Implementation

The model implementation developed for cell segmentation includes three main steps: training the Cellpose model, evaluating it on labeled data, and testing on new, unsegmented data in a Google Colab workspace (GPU required). It integrates the original Cellpose notebook [4], a notebook from [5], and custom modifications such as dynamic diameter adjustments, format specifications, and an extended evaluation metric for cellwise Dice Score calculation.

The dynamic calculation of the average pixel diameter, based on image dimensions, improves segmentation performance. In the presented dataset, an image with dimensions `1200x1600` typically contains a RBC with a diameter of 45 pixels, while a scaled `600x800` image (0.5 scaling) contains cells with a diameter of 22.5 pixels. This adjustment

enhances segmentation as RBCs have relatively consistent diameters [10]. Figure 2 compares segmentation results of a fixed diameter (left) and dynamic adjustment calculation (right).

Fig. 2: Impact of average cell diameter on segmentation results
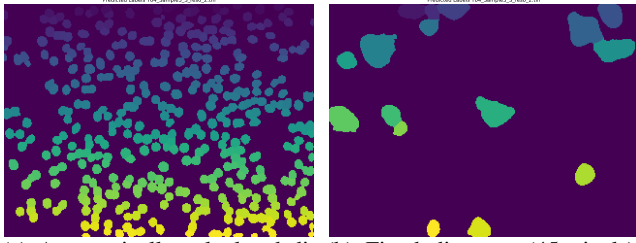
(a) Automatically calculated diameter (9 pixels) based on image resolution (0.2). The segmentation accurately reflects cell sizes.

(b) Fixed diameter (45 pixels), independent of image resolution. This results in inaccurate segmentation.

G. Experimental Design

Experiments involved training *Model 1* on 60 images and masks (2 samples per mode) and *Model 2* on 150 images and masks (5 samples per mode). The evaluation dataset consisted of 360 images and masks (5 samples per mode, 24 scaling levels). Training parameters are detailed in Table III.

TABLE III: Training and Testing Summary for Model 1 and Model 2

Parameter	Model 1: 2 Samples	Model 2: 5 Samples
Pretrained Model	cyto3	cyto3
Epochs	100	100
Diameter of Labels	24.32	23.56
Training Masks	60	150
Testing Masks	60	150
Final Training Loss	0.9477	0.8473

H. Evaluation Metrics

Segmentation performance was evaluated at *pixel-* and *cell-level* using a Dice threshold of 0.8 to classify cells as True Positives (TP) or False Positives (FP). Metrics include the Panoptic Quality (PQ) score, F1 Score, and Precision. The PQ score combines quality and quantity of cell detections:

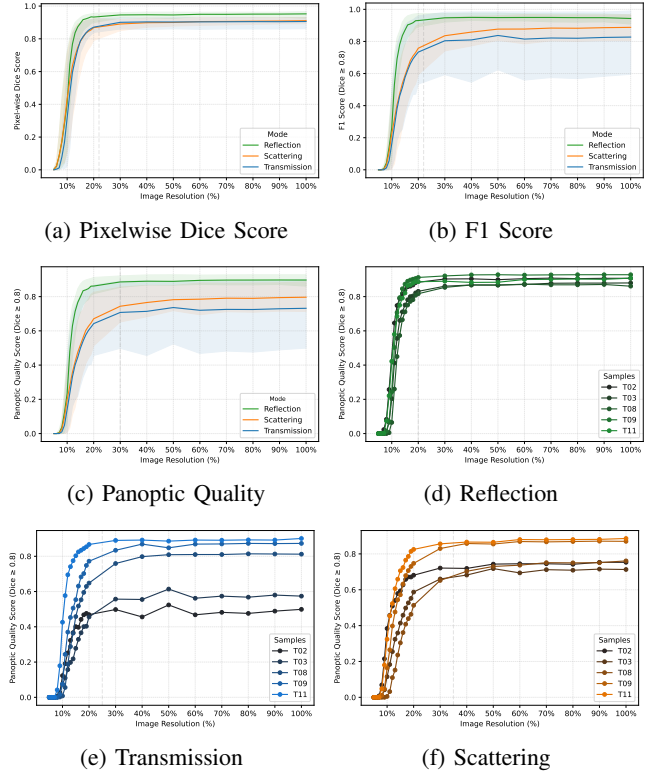$$PQ = \frac{|TP|}{|TP| + 0.5 \cdot (|FP| + |FN|)}$$

IV. RESULTS

The two trained Cellpose models (using 2 vs. 5 samples) produced identical results on the Evaluation Data I. Table IV shows the evaluation for T02_Sample1 in reflection mode. At full size `1200x1600`, the model correctly segmented 624 out of 634 cells, achieving a Dice Score of 0.965 when the full image was treated as a binary mask. At 10% resolution, only one cell out of 629 was correctly segmented. Figure 3 shows that the pixelwise Dice score remains above 0.8 until the image resolution is reduced to 20% of the original resolution

(Figure 3a), and the F1 Score and PQ stay above 0.7 until the image resolution is reduced to 30% of the original resolution (Figure 3b and 3c). Significant variation in performance is seen, especially in transmission mode (Figure 3e). The model performs best in reflection mode, followed by transmission and scattering (Figure 3d to 3f).

TABLE IV: Evaluation Metrics for T02_Sample1_Reflection

Resolution	Dice	PQ	TP	FP	FN	F1	#GT	#Pred
100%	0.965	0.908	598	26	36	0.958	634	624
90%	0.963	0.908	597	23	37	0.963	634	620
80%	0.963	0.907	597	24	37	0.961	634	621
70%	0.963	0.910	597	18	37	0.971	634	615
60%	0.963	0.909	596	18	38	0.971	634	614
50%	0.958	0.902	588	17	46	0.972	634	605
40%	0.960	0.904	591	18	43	0.970	634	609
30%	0.959	0.901	590	17	44	0.972	634	607
20%	0.938	0.856	556	20	78	0.965	634	576
10%	0.012	0.000	0	1	629	0.000	629	1

Fig. 3: Evaluation of metrics across five samples (T02, T03, T08, T09, T11) at varying resolutions and modalities

(a) Pixelwise Dice Score

(b) F1 Score

(c) Panoptic Quality

(d) Reflection

(e) Transmission

(f) Scattering

In Figure 4, T02_Sample1_R is segmented at four resolutions. At 15% resolution (Figure 4c), the pixelwise Dice score is 0.924, but the cell outlines are jagged. At 10%, the round shape of the cells is lost, and none of the RBCs are correctly segmented, with the ground truth mask showing only rectangular "cells."

A. Final Testing

Using the *Model 2*, segmentation masks were generated for the test dataset. Two examples for resolutions 70% and 20%

Fig. 4: Ground truth and prediction overlays at different resolutions (1x, 0.5x, 0.15x, 0.1x) - T02_Sample1_R

(a) 100%

(b) 50% of original resolution

(c) 15% of original resolution

(d) 10% of original resolution
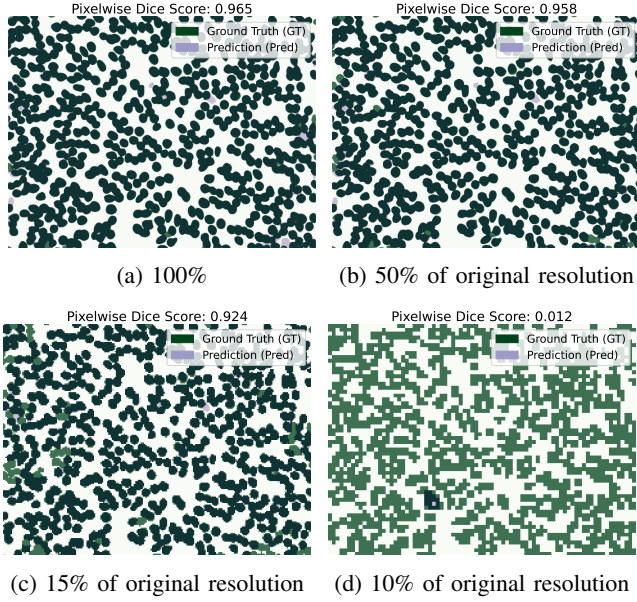
are shown in Figure 5. At 70% resolution, the outlines of the cells are clearly detected, and even half edge cells are identified. In Figure 5b most of the cells are still recognized, though in the lower right corner, the model struggles to identify the bright overlapping cells. The outlines, compared to the 70% resolution, appear more jagged.

Fig. 5: Segmentation on unknown test samples

(a) T07_Sample1_R - 70% of original image resolution

(b) T07_Sample1_R - 20% of original image resolution
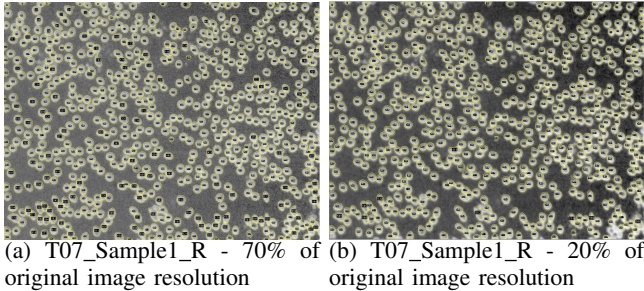
V. Discussion

a) Dataset Quality and Improvement: Unclear cell boundaries in several samples affect segmentation. A higher-quality dataset with better-defined boundaries would improve cellpose model training. Testing and Training on other datasets could enhance model robustness.

b) Choice of DL Segmentation Algorithm: Cellpose 2.0 [20] is used in this study, but the DL-model like Mask R-CNN could perform better for the Toy2 dataset, given its suitability for similar-looking cells [13]. Further comparison is needed.

c) Cellpose Model Training: Training with more Toy2 and Toy1 dataset samples would improve results. It is surprising that *Models 1 and 2* produce identical results. Testing the "Human-in-the-Loop" feature from Cellpose 2 could refine the model [20].

d) Ground Truth Mask Creation: GT masks were created by one person. Multiple contributors should generate masks, and averages should be used. The bias introduced by using reflection mode should be considered, as it produces the best results.

VI. Conclusion

Malaria is a major global health threat, particularly in sub-Saharan Africa and Southeast Asia, where limited access to fast and reliable diagnostic tools is a critical issue. Advances in image analysis and deep learning algorithms offer promising solutions to address the limitations of conventional malaria diagnosis methods. Merdasa et al. propose an approach that employs three imaging modes, eliminating the need for labor-intensive staining methods [16]. Instead, a multimodal and multispectral analysis distinguishes between different stages of malaria parasites effectively [16].

This study explores the impact of reduced image resolution on the accuracy of cell segmentation. Two Cellpose models are trained on a subset of the Toy2 dataset [7] using manually created ground truth masks. The segmentation performance is evaluated from `1200x1600` to `60x80` pixels using Dice, F1, and Panoptic Quality Scores at both the pixel and cell levels.

The analysis identifies that segmentation accuracy remains consistent at resolutions as low as `360x480` pixels (30% of the original resolution) and gradually declines beyond this threshold. Images smaller than `180x240` pixels (15% of the original resolution) fail to deliver satisfactory results. In particular, the smoothness of cell outlines deteriorates significantly as resolution decreases, especially below 30% of the original image size. Among the imaging modes, the reflection mode outperforms the transmission and scattering modes in segmentation accuracy, possibly due to the GT masks being generated based on the reflection mode. The complete code is publicly available for replication and further research at https://github.com/dernno/Multimodal-RBC-Segmentation.git.

A. Future Work

In future research, a systematic evaluation is needed to determine whether Cellpose is the most suitable DL segmentation algorithm for the Toy2 dataset or if models like Mask R-CNN perform better. Expanding the dataset and generating separate ground truth masks for transmission and scattering modes may enhance robustness and segmentation quality. By improving accuracy and reliability of red blood cell segmentation, this research significantly contributes to reducing malaria misdiagnoses.

Acknowledgment

REFERENCES

[1] W. Abdulla, "Mask R-CNN for object detection and instance segmentation on Keras and TensorFlow," 2017. [Online]. Available: https://github.com/matterport/Mask_RCNN.

[2] C. Y. Bae et al., "Embedded-deep-learning-based sample-to-answer device for on-site malaria diagnosis," Front. Bioeng. Biotechnol., vol. 12, Jul. 2024, doi: 10.3389/fbioe.2024.1392269

[3] M. Brydegaard, A. Merdasa, H. Jayaweera, J. Ålebring, and S. Svanberg, "Versatile multispectral microscope based on light emitting diodes," Review of Scientific Instruments, vol. 82, no. 12, p. 123106, Dec. 2011, doi: 10.1063/1.3660810

[4] Cellpose Team. *Cellpose Code*. Available at: https://colab.research.google.com/github/MouseLand/cellpose/blob/main/notebooks/run_cellpose_2.ipynb.

[5] Sreenu, B. N. *Python for Microscopists: Cellpose Algorithm for Segmentation*. Available at: https://github.com/bnsreenu/python_for_microscopists/blob/master/305_What_is_Cellpose_algorithm_for_segmentation.ipynb.

[6] H. A. H. Chaudhry, M. S. Farid, A. Fiandrotti, and M. Grangetto, "A lightweight deep learning architecture for malaria parasite-type classification and life cycle stage detection," Neural Comput & Applic, vol. 36, no. 31, pp. 19795–19805, Nov. 2024, doi: 10.1007/s00521-024-10219-w

[7] Toy2. Multispectral Dataset. Acquired using a multispectral light-emitting diode microscope.

[8] A. Dev, M. M. Fouda, L. Kerby, and Z. Md Fadlullah, "Advancing Malaria Identification From Microscopic Blood Smears Using Hybrid Deep Learning Frameworks," IEEE Access, vol. 12, pp. 71705–71715, 2024, doi: 10.1109/ACCESS.2024.3402442 .

[9] S. Doumun OULAI, S. Dabo-Niang, and J. Zoueu, "A Multispectral Blood Smear Background Images Reconstruction for Malaria Unstained Images Normalization," International Journal of Imaging Systems and Technology, vol. 34, no. 6, p. e23182, 2024, doi: 10.1002/ima.23182

[10] D. A. Fedosov, B. Caswell, and G. E. Karniadakis, "A Multiscale Red Blood Cell Model with Accurate Mechanics, Rheology, and Dynamics," *Biophysical Journal*, vol. 98, no. 10, pp. 2215-2225, 2010. [Online]. Available: https://www.sciencedirect.com/science/article/pii/S0006349510002286.

[11] D. Franco-Barranco, A. Muñoz-Barrutia, and I. Arganda-Carreras, "Stable Deep Neural Network Architectures for Mitochondria Segmentation on Electron Microscopy Volumes," Neuroinformatics, vol. 20, no. 2, pp. 437–450, Apr. 2022, doi: 10.1007/s12021-021-09556-1 .

[12] B. Goh et al., "The application of spectroscopy techniques for diagnosis of malaria parasites and arboviruses and surveillance of mosquito vectors: A systematic review and critical appraisal of evidence," PLoS Neglected Tropical Diseases, vol. 15, no. 4, p. e0009218, Apr. 2021, doi: 10.1371/journal.pntd.0009218 .

[13] K. He, G. Gkioxari, P. Dollár, and R. Girshick, "Mask R-CNN," arXiv:1703.06870 [Titel anhand dieser ArXiv-ID in Citavi-Projekt übernehmen] [cs], Jan. 2018. [Online]. Available: https://arxiv.org/abs/1703.06870.

[14] P. Lebel, R. Dial, V. N. P. Vemuri, V. Garcia, J. DeRisi, and R. Gómez-Sjöberg, "Label-free imaging and classification of live P. falciparum enables high performance parasitemia quantification without fixation or staining," PLoS Comput Biol, vol. 17, no. 8, p. e1009257, Aug. 2021, doi: 10.1371/journal.pcbi.1009257 .

[15] Z. Liang et al., "CNN-based image analysis for malaria diagnosis," in 2016 IEEE International Conference on Bioinformatics and Biomedicine (BIBM), Shenzhen, China: IEEE, Dec. 2016, pp. 493–496, doi: 10.1109/BIBM.2016.7822567 .

[16] A. Merdasa, M. Brydegaard, S. Svanberg, and J. T. Zoueu, "Staining-free malaria diagnostics by multispectral and multimodality light-emitting-diode microscopy," J Biomed Opt, vol. 18, no. 3, p. 036002, Mar. 2013, doi: 10.1117/1 .JBO.18.3.036002 .

[17] M. S.-D. Mora, "Malaria-Transmission-Diagnosis and Treatment," in Malaria - Transmission, Diagnosis and Treatment, IntechOpen, 2023. doi: 10.5772/intechopen.113746 .

[18] D. L. Omucheni, K. A. Kaduki, W. D. Bulimo, and H. K. Angeyo, "Application of principal component analysis to multispectral-multimodal optical image analysis for malaria diagnostics," Malar J, vol. 13, p. 485, Dec. 2014, doi: 10.1186/1475-2875-13-485 .

[19] S. Doumun Oulai, S. Dabo-Niang, and J. Zoueu, "A Multispectral Blood Smear Background Images Reconstruction for Malaria Unstained Images Normalization," *International Journal of Imaging Systems and Technology*, vol. 34, no. 6, p. e23182, 2024, doi: 10.1002/ima.23182 .

[20] M. Pachitariu and C. Stringer, "Cellpose 2.0: how to train your own model," *Nature Methods*, vol. 19, no. 12, pp. 1634–1641, Dec. 2022, doi: 10.1038/s41592-022-01663-4 .

[21] "Malaria - PAHO/WHO — Pan American Health Organization." Accessed: Dec. 29, 2024. [Online]. Available: https://www.paho.org/en/topics/malaria.

[22] M. Poostchi, K. Silamut, R. J. Maude, S. Jaeger, and G. Thoma, "Image analysis and machine learning for detecting malaria," Transl Res, vol. 194, pp. 36–55, Apr. 2018, doi: 10.1016/j.trsl.2017.12.004 .

[23] U. Schmidt, M. Weigert, C. Broaddus, and G. Myers, "Cell detection with star-convex polygons," in *Medical Image Computing and Computer Assisted Intervention - MICCAI 2018 - 21st International Conference, Granada, Spain, September 16-20, 2018, Proceedings, Part II*, 2018, pp. 265–273.

[24] Uwe Schmidt, Patrick Köhler, and others, "StarDist: Matching Implementation," 2021, https://github.com/stardist/stardist/blob/main/stardist/matching.py. Accessed: 2024-12-30.

[25] C. Stringer, M. Michaelos, and M. Pachitariu, "Cellpose: a generalist algorithm for cellular segmentation," Feb. 03, 2020, bioRxiv. doi: 10.1101/2020.02.02.931238 .

[26] N. J. White, "Severe malaria," Malar J, vol. 21, no. 1, Art. no. 1, Dec. 2022, doi: 10.1186/s12936-022-04301-8 .

[27] World Health Organization, "Fact sheet about malaria," 2024. [Online]. Available: https://www.who.int/news-room/fact-sheets/detail/malaria. Accessed: Dec. 29, 2024.